The Astrophysical Journal, 600:141–148, 2004 January 1

LARGE-FIELD MULTICOLOR STUDY OF A168: SUBCLUSTERS, DYNAMICS, AND LUMINOSITY FUNCTIONS

Yanbin Yang,[1] Xu Zhou,[1] Qirong Yuan,[1,2] Zhaoji Jiang,[1] Jun Ma,[1] Hong Wu,[1] and Jiansheng Chen[1]

Received 2003 May 8; accepted 2003 September 9

ABSTRACT

This paper presents a multicolor study of the nearby cluster of galaxies A168 ($z = 0.045$) with 13 intermediate-band filters in the Beijing-Arizona-Taiwan-Connecticut (BATC) filter system. After a cross-identification between the photometric data obtained from the BATC and the Sloan Digital Sky Survey (SDSS), a catalog containing 1553 galaxies down to $r' < 20.0$ mag is achieved, which includes 121 spectroscopically confirmed member galaxies. The technique of photometric redshift has been applied to all these galaxies with combined 18 band (13 from BATC and five from SDSS) spectral energy distributions (SEDs), in order to perform a faint membership selection in A168. As a result, 255 galaxies are newly selected as the member candidates. On the basis of the enlarged sample of cluster galaxies, the spatial distribution and dynamics of A168 are investigated. In light of the spatial distribution of the member galaxies and the 0.2–3.5 keV X-ray image by the *Einstein X-Ray Observatory*, it seems that A168 consists of two merging subclusters with a relative radial velocity of 264 ± 142 km s^{-1}. With the help of ROSTAT software, a detailed investigation of the dynamics shows the intrinsic difference in the velocity distributions for these two subclusters. Under a linear two-body model, they are found to be a gravitationally bound system with 92% probability. The slight deviation of the local velocity distribution from the overall distribution in the central region may suggest a picture of head-on collision in the projection plane. By using a *double* Schechter function, the close examination of the luminosity functions reveals the different galaxy content of these two subclusters, which implies that the merging process is possibly at the early stage.

Subject headings: galaxies: clusters: individual (A168) — galaxies: distances and redshifts — galaxies: kinematics and dynamics — galaxies: luminosity function, mass function

1. INTRODUCTION

The increasing volume of observational data for galaxy clusters (GCs) in multiple wavebands provides important constraints on the formation of large-scale structures and cosmology (Bahcall 1988; Dressler & Gunn 1988; Schindler 2001). The investigations of the luminosity function and the spectral features of member galaxies in a rich cluster will help us to understand not only the structures and dynamics of the whole galaxy cluster but also the formation and evolution of galaxies under such a dense environment (Dressler 1984; Poggianti 2002).

Spectroscopic observation in the optical band is still the most straightforward and powerful approach to membership determination. However, reliable spectroscopy for the faint galaxies in a cluster is still an unattainable goal for large telescopes. With the development of the photometric redshift technique, the redshifts of faint galaxies can be significantly determined according to their spectral energy distributions (SEDs). The Beijing-Arizona-Taiwan-Connecticut (BATC) sky survey is specially designed for this purpose. In this paper we present a large-field multicolor study of the galaxy cluster A168 based on the BATC observations with 13 intermediate-band filters, which covers the whole optical band. Improvement of the accuracy of the photometric redshift estimate with our multicolor system allows us to study the spatial and the dynamic properties of the nearby clusters of galaxies (Yuan et al. 2001, 2003).

A168 is a nearby ($z = 0.045$) cluster of galaxies located at $01^{\rm h}15^{\rm m}10\overset{\rm s}{.}2, +00^\circ12'18''$ (J2000.0) with richness of II–III (BM classification). Its distance modulus is 36.45 by assuming $q_0 = 0.5$ and $H_0 = 75$ km s^{-1} Mpc^{-1} (also used throughout this paper). The luminosity function of A168 was remarked as the best example of non-Schechter form by Dressler (1978), which was confirmed by Oegerle, Ernst, & Hoessel (1986). On the basis of the positional discrepancy of $\sim 10'$ (i.e., ~ 540 kpc) between the X-ray and the optical center, Ulmer, Wirth, & Kowalski (1992) suggested that A168 was formed by the collision of two clusters with approximately equal sizes. It is reported that the X-ray emission of A168 has two peaks with surface brightnesses of 9×10^{-14} and 3×10^{-14} ergs s^{-1} cm^{-2}, respectively (Tomita et al. 1996). They supposed that the star-forming processes will be triggered when gas-rich galaxies rush into the higher density regions. However, Tomita et al. (1996) failed to find the enhanced fraction of blue galaxies in the region between these two X-ray peaks.

This paper aims at not only selecting faint member galaxies of A168 by the photometric redshift technique, but also investigating the substructures in the spatial distribution and the line-of-sight velocity distributions. We wish to provide direct evidence of the ongoing merger event of A168 from our analysis of multicolor photometries. This paper is structured as follows: In § 2, we describe the BATC observations and the data reduction. The technique of photometric redshift is used to estimate the redshift for all galaxies; then the membership selection of A168 is performed. In § 3, the substructures of

[1] National Astronomical Observatories, Chinese Academy of Sciences, Beijing 100012, People's Republic of China; yyb@bac.pku.edu.cn, zhouxu@bac.pku.edu.cn.

[2] Department of Physics, Nanjing Normal University, NingHai Road 122, Nanjing 210097, People's Republic of China.

A168 are explored on the basis of the member galaxy distribution and the X-ray emission of hot gas. The dynamics of substructures are also studied. In § 4 the luminosity functions (LFs) of A168 are analyzed. The summary is given in § 5.

2. DATA

2.1. *BATC Observation and Data Reduction*

The BATC program is a large-field ($58' \times 58'$) multicolor sky survey based on the 60/90 cm f/3 Schmidt Telescope of National Astronomical Observatories, Chinese Academy of Sciences (NAOC). A Ford Aerospace 2048×2048 CCD camera with a pixel size of 15 μm ($\sim 1\farcs7$ pixel^{-1}) is mounted on the telescope. The BATC filter system contains 15 intermediate-band filters (Fig. 1) covering a wavelength range from 3000 to 10000 Å, which are specifically designed for avoiding night-sky emission lines. A detailed description of the BATC photometric system can be found in Fan et al. (1996) and Zhou et al. (2003).

From 1995 August to 2002 March, we totally accumulated about 37 hours of exposure for A168 with 13 filters. More information about our observations is given in Table 1. The raw data are processed with an automatic data reduction software named PIPELINE I (Fan et al. 1996), which includes bias subtraction and dome flat-field correction. The technique of integral pixel shifting is used in the image combination during which the cosmic rays and bad pixels are corrected by comparing multiple images. The mean error of position calibration is $\sim 0\farcs5$ by taking the Guide Star Catalog (GSC) as standard. By using the PIPELINE II software (Zhou et al. 2003), developed on the basis of the DAOPHOT kernel, photometries are performed for all the objects detected. As a result, the photometries with the point-spread function (PSF) model and the different apertures are obtained for 4798 objects detected in at least three bands. The flux calibration of the SEDs is performed by using the Oke-Gunn standard stars that were observed during photometric nights. Detailed information about calibration can be found in Zhou et al. (2001). Because we have no calibration image for the g filter, we instead perform a model calibration that is specially developed for the large-field photometric system by Zhou et al. (1999).

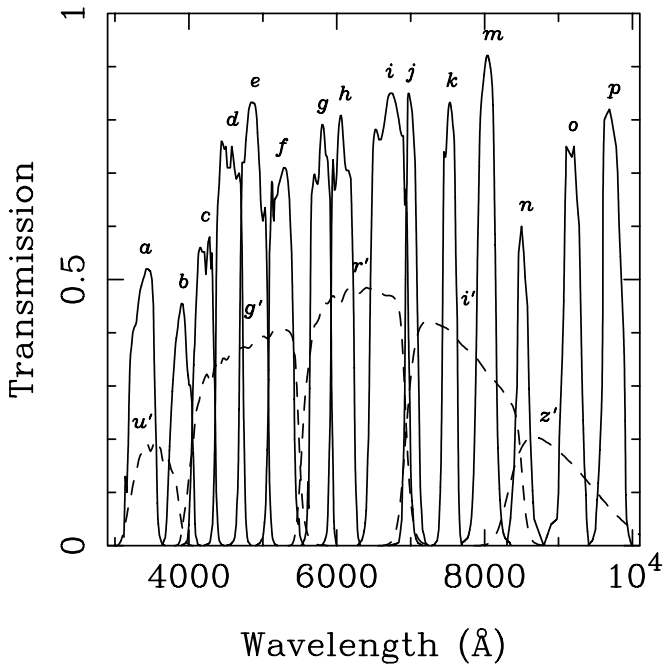

FIG. 1.—Transmission curves of filters in the BATC (*solid lines*) and the SDSS (*dashed lines*) photometric system. The names of the filters are marked at the top of each curve.

TABLE 1

PARAMETERS OF THE BATC FILTERS AND THE STATISTICS OF THE OBSERVATIONS OF A168

Number (1)	Filter (2)	$\lambda_{\rm eff}$ (Å) (3)	FWHM (Å) (4)	Exposure (hr) (5)	N_1[a] (6)	Seeing[b] (arcsec) (7)	N_2[c] (8)
1.....	*c*	4210	309	3.67	11	5.08	1
2.....	*d*	4546	332	5.33	16	4.09	1
3.....	*e*	4872	374	4.00	12	3.94	2
4.....	*f*	5250	344	3.47	11	4.18	4
5.....	*g*	5785	289	1.33	4	3.81	0
6.....	*h*	6075	308	1.00	3	4.80	3
7.....	*i*	6710	491	1.08	4	3.80	3
8.....	*j*	7010	238	2.00	6	3.94	1
9.....	*k*	7530	192	2.00	6	4.49	3
10.....	*m*	8000	255	5.67	17	3.94	1
11.....	*n*	8510	167	2.67	8	4.81	2
12.....	*o*	9170	247	1.33	4	6.29	1
13.....	*p*	9720	275	3.40	11	5.03	2

[a] Number of images of each color.
[b] The seeing is of the combined images.
[c] Number of calibration images.

2.2. *Combining the BATC and the SDSS SEDs of galaxies*

A168 has been observed by SDSS with five broad bands, namely u', g', r', i', z' (Fig. 1) , and the photometric data are distributed in the SDSS Early Data Release (EDR; see Stoughton et al. 2002). The method of combining the SDSS photometric data and the BATC SEDs is explored recently by Yuan et al. (2003), and this work shows that the combined SEDs could lead to a more accurate estimate of photometric redshifts. We cross-identify the BATC source list with the SDSS photometric catalog in the same region, and a catalog containing 2580 galaxies and 2218 stars is achieved. The object classifications are taken from the result of SDSS photometries. For the photometries of BATC, we adopt the PSF magnitudes for stars and take a fixed aperture with a radius of 4 pixels (i.e., $r_{\rm ap} \sim 6\farcs8$) for galaxies. In order to combine the photometric results of the BATC and the SDSS, an aperture correction should be applied to the SDSS model magnitudes ($m_{\rm model}$) by

$$\Delta m = m_{\rm ap} - m_{\rm model} = -2.5 \log \frac{\int_0^{r_{\rm ap}} 2\pi r I(r) dr}{\int_0^{\infty} 2\pi r I(r) dr} , \quad (1)$$

where $m_{\rm ap}$ is the aperture magnitude and $I(r)$ is the preferred profile function of surface intensity (e.g., the power-law or de Vaucouleurs $r^{1/4}$ model). The model magnitude in each band and its corresponding parameters that are used to quantify the preferred brightness profile can be found in the SDSS data.

To observe the possible systematic offset between the BATC and the SDSS photometric system, we derive the zero-point difference of the SEDs (ZPDS) for each object by calculating the difference between the SDSS r' magnitude and the interpolated BATC magnitude at 6180 Å. Figure 2 shows the distribution of ZPDSs for all the objects detected. For

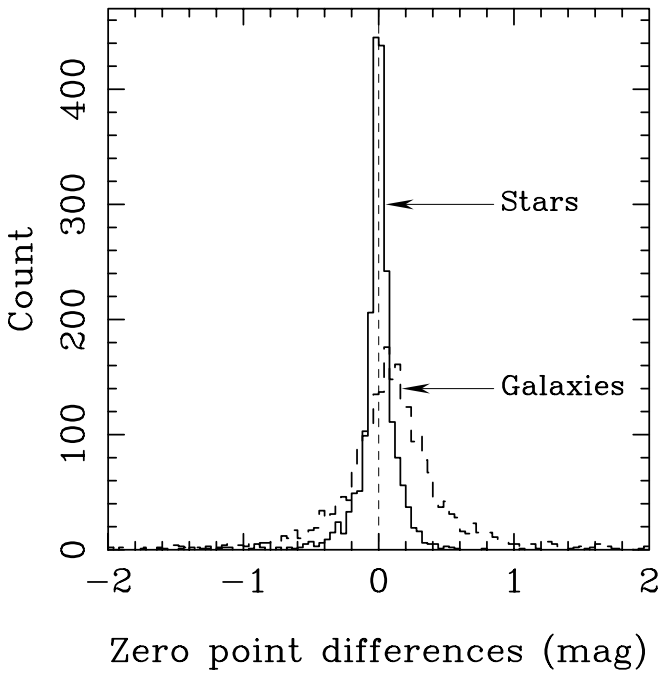

FIG. 2.—Histogram of the zero-point differences of individual SEDs in the BATC system and the SDSS system for all galaxies and stars.

stars, the magnitude offset between these two photometric systems approximates to zero, indicating that the BATC and SDSS photometric systems are in good agreement. For galaxies, a more widely spread distribution of ZPDSs is found. This might be the result of the errors in photometries and the uncertainties in model fittings. For adapting to the BATC multicolor photometric system, the SDSS SEDs are corrected by adding their ZPDS. Finally, we obtain the combined SEDs, including 13 BATC bands plus five SDSS bands, for 1553 galaxies brighter than $r' = 20$ mag.

2.3. *Photometric Redshift and Membership Determination*

The photometric redshift technique was originally developed for detecting high-z objects on the basis of the broadband photometries (Pelló et al. 1999; Bolzonella, Miralles, & Pelló 2000). The 15 intermediate-band SEDs obtained by the BATC photometric system can be regarded as the rough spectrum. The advantages of the BATC data in measuring the photometric redshift of some faint galaxies can be expected. With the BATC SEDs (Yuan et al. 2001; Xia et al. 2002) and the combined SEDs of the BATC and the SDSS (Yuan et al. 2003), the photometric redshifts of faint galaxies can be estimated with a certain accuracy ($\Delta z_{\rm phot} \approx 0.02$), which allows us to isolate the member galaxies for some nearby galaxy clusters.

The technique of photometric redshift has been applied to the 18 band SEDs with the help of the Hyperz code (Bolzonella et al. 2000). The redshifted spectral templates of normal galaxies are used to fit the observed SEDs, and the reddening law is set to be a free parameter during the fitting. The photometric redshift for each galaxy is searched in a redshift range from 0.0 to 1.0, with a searching step of 0.005. The histogram of $z_{\rm phot}$ for all galaxies is plotted in Figure 3, and most of them are located at $z < 0.5$. A total of 195 galaxies with known spectroscopic redshifts $z_{\rm spec} < 0.25$ are

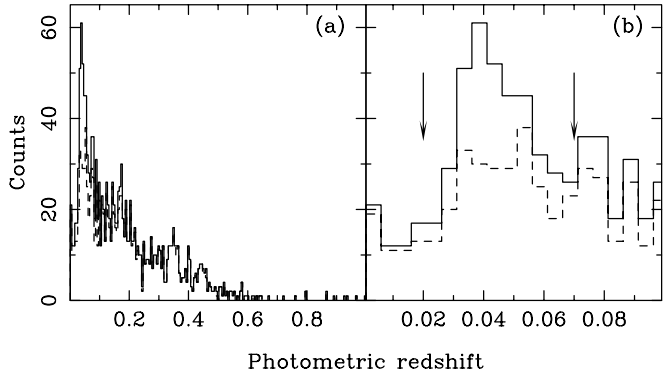

FIG. 3.—(*a*) Histogram of photometric redshift for 1553 galaxies. The distribution from 0.0 to 0.1 is shown enlarged in (*b*). In both figures, the solid lines represent photometric redshifts of all galaxies, and the dashed lines indicate photometric redshifts of the galaxies without spectroscopic redshift. The range of [0.02, 0.07] marked by two arrows is taken as the criterion for member candidates.

selected to derive the uncertainty of the photometric redshift, which is found to be ~ 0.024 (see Fig. 4).

According to the known spectroscopic redshifts, there are 121 galaxies distributed in a range from 0.04 to 0.05. We take them as the member galaxies of A168. About 90% (109/121) galaxies have photometric redshifts within the range [0.02, 0.07]; thus we take this range as the criterion for the membership determination based on the photometric redshift. As a result, 255 galaxies are selected as the member candidates. Together with the spectroscopically confirmed members, we obtain an enlarged sample of 376 member galaxies in total. It should be noted that the uncertainty of photometric redshift is rather large compared with the intrinsic dispersion of A168, but it still can be used to select the

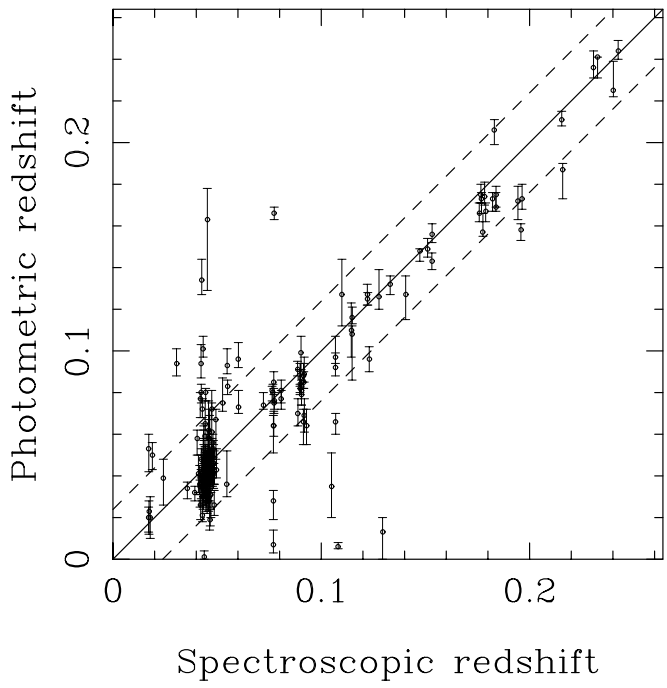

FIG. 4.—Comparison of photometric redshifts and spectroscopic redshifts for 195 known galaxies. The dashed lines mark the $2\,\sigma$ region of the photometric redshifts.

member galaxy candidates with high efficiency, especially for the faint galaxies.

3. SUBSTRUCTURES

3.1. *Spacial Distribution of Members and X-Ray Map*

Figure 5 gives the spatial distribution of 376 member galaxies (*small circles*), with its corresponding contour map (*thin lines*) of the number density superposed. In the figure, D indicates the density peak located at $01^h15^m06^s$, $+00^\circ19'12''$ (J2000.0). The spatial distribution is elongated along the northwest-southeast direction with a position angle of $\sim 30^\circ$. A possible group (A168WG), indicated by E in the figure, can be recognized to the west of the cluster core. The group is close to the high-density region and seems to be falling toward the center, increasing the galaxy density there. A similar spatial distribution was earlier derived by Kriessler & Beers (1997), but their sample of 106 galaxies did not show the core structures and the group clearly. We take the density peak as the center and then derive the radial number density profile in Figure 6. It is clear that most of the galaxies are concentrated within a range of about $12'$ (~ 0.7 Mpc).

The X-ray image in 0.2–3.5 keV band, observed by IPC of the *Einstein X-Ray Observatory*, is overlaid on the spatial distribution in Figure 5 (*thick lines*). It is interesting that the X-ray map and the member distribution coincide well with each other in both their spatial locations and their shapes. As mentioned above (§ 1), the X-ray emission of A168 has two peaks, marked by A and B in Figure 5. The higher X-ray peak, point A, is located at $01^h14^m57^s$, $+00^\circ25'04''$ (J2000.0) with a distance of $\sim 6'$ (i.e., ~ 320 kpc) to the density peak. In the figure, C points to the cD galaxy UGC 00797. Point A is very close to the cD galaxy, which agrees with the traditional experience that D/cD galaxies are located around the peak of the X-ray emission (Jones et al. 1979; Forman & Jones 1982). However, this cD galaxy significantly deviates from the local density peak of A168, which seems inconsistent with the idea that a D/cD galaxy appears to be associated with the center of its host cluster (Beers & Geller 1983; Oegerle & Hill 2001). On the other hand, the lower X-ray peak, point B, is surrounded by the clustering bright galaxies. From the shape of the X-ray emission, the hot gas between the two peaks seems to be pushed away from the center by the head-on collision of the two clumps. Combining all the above characteristics, it seems that there are some substructures in A168. Ulmer et al. (1992) pointed out that A168 was possibly formed by the collision of two subclusters. If this is true, it is reasonable to assume that the collision occurs along the elongated direction. To explore the substructures in detail, we artificially divide the main region of A168 (indicated by a $0.^\circ4 \times 0.^\circ6$ box in Fig. 5) into two equal parts. One is centered at the higher X-ray peak with 79 galaxies. We call it the north subcluster (A168N). Another is located at the lower X-ray peak with 97 galaxies, called the south subcluster (A168S). In the following sections we try to find other evidence to support the idea that they are indeed physically different parts in A168; in other words, they are really two subclusters, and we will show that they seem to be under a merging process.

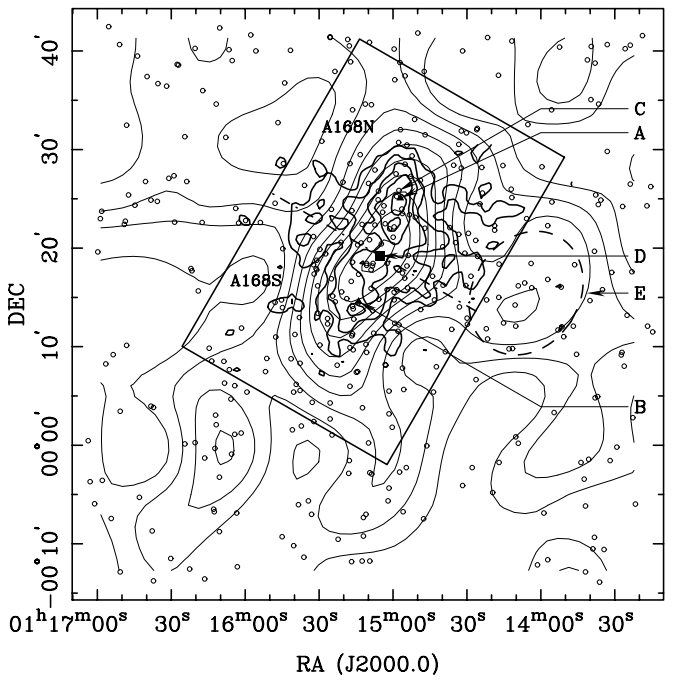

FIG. 5.—Member distribution (*small circles*) of A168, with corresponding contour map superposed (*thin lines*). Thick lines represent the contour map of the X-ray image. Point A and point B are the two X-ray peaks. C points to the cD galaxy UGC 00797. D points to the number density peak. E points to the possible west group indicated by a dashed line ellipse. The box ($0.^\circ4 \times 0.^\circ6$) indicates the central region of the cluster. The dot-dashed line divides the north subcluster (A168N) and the south subcluster (A168S) equally (see § 3 for detailed analysis).

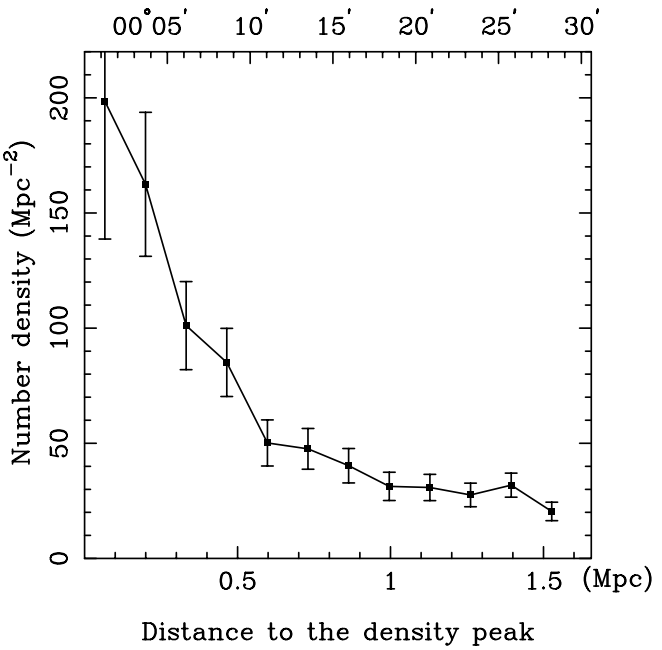

FIG. 6.—Radial number density profile. The bottom abscissa shows the distance in units of Mpc. The top abscissa is in units of arcminutes.

3.2. *Dynamics of Substructures*

Provided that A168 is formed by merging of two subclusters, the dynamics remaining after the collision should be presented by testing the velocity distribution. On the basis of the spectroscopically confirmed member galaxies, we are able to study the dynamics of A168 in detail. The statistical parameters of A168N, A168S, A168WG, and A168 are listed in Table 2. The mean redshift (z), the mean velocity (v_r), and the velocity dispersion (σ_r) are all calculated by the biweight statistic in ROSTAT software (Beers, Flynn, & Gebhardt 1990), except

TABLE 2
PARAMETERS OF A168

Parameter	A168N	A168S	A168WG	A168
N_{gal}[a]	79	97	19	376
$N_{gal,spec}$[b]	26	52	6	121
z	0.0446 ± 0.0004	0.0455 ± 0.0003	0.0466 ± 0.0001	0.0451 ± 0.0002
v_r (km s^{-1})	13065 ± 113	13329 ± 86	13633 ± 35	13206 ± 50
σ_r (km s^{-1})	564 ± 90	613 ± 56	491 ± 189	554 ± 34
$\langle 1/r_p \rangle^{-1}$ (Mpc)[c]	0.30	0.30	...	0.77
M (10^{14} $M_\odot$)	2.1 ± 0.7	2.5 ± 0.5	...	5.2 ± 0.6
AI[d]	−0.263	−0.392	−0.327	−0.093
TI[e]	1.458	0.958	0.000	0.901

NOTE.—The errors are computed at the 68% confidence level.
[a] The number of galaxies including the spectroscopically confirmed members and the photometric redshift selected candidates.
[b] The number of galaxies including only the spectroscopically confirmed members.
[c] Gravitational scale length.
[d] Asymmetry index.
[e] Tail index.

that the velocity dispersion of A168WG is taken from the gapping statistic. The asymmetry index (AI) and the tail index (TI) of the velocity distributions are also provided by ROSTAT. Figure 7 shows the velocity distribution of these two subclusters. The distribution of A168N is more concentrated than that of A168S. It seems that, for A168S, there is a gap at $\sim$ 13,000 km s^{-1}, which can be clearly seen from a stripe density plot in Figure 8. According to the value of TI (see Bird & Beers 1993 for detail), A168N possesses a light-tailed distribution, while the distribution of A168S is nearly Gaussian. This suggests that these two distributions are intrinsically different. Moreover, the classical Kolmogorov-Smirnov (K-S) test also shows that the velocity distributions of these two subclusters are from the different parent distributions with 94% probability.

Although the interaction between these two subclusters appears obvious according to the spatial distribution, one should keep in mind this is a projection effect. So it is necessary to estimate the probability that they are gravitationally bound, in order to confirm that they are really two interacting subclusters. We take a linear two-body model for the system as Beers, Geller, & Huchra (1982) did in analyzing

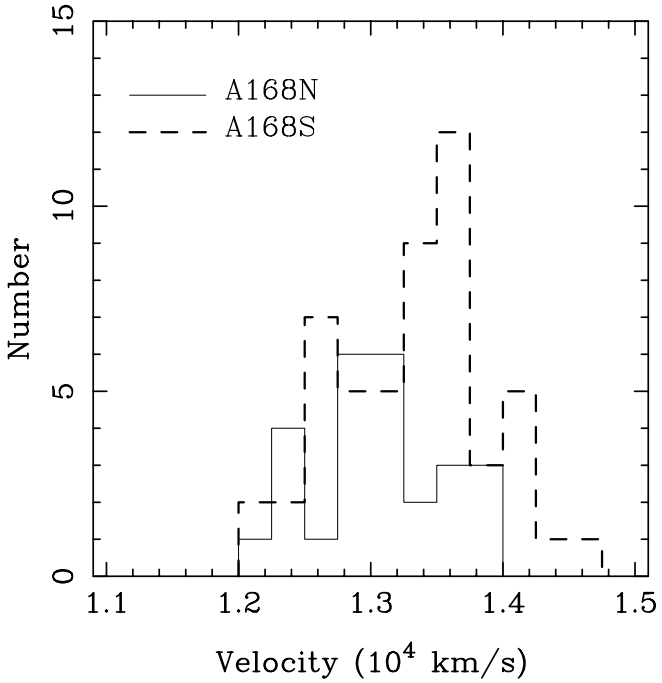

FIG. 7.—Velocity distributions of the spectroscopically confirmed member galaxies for A168N and A168S are presented by the solid line and the dashed line, respectively.

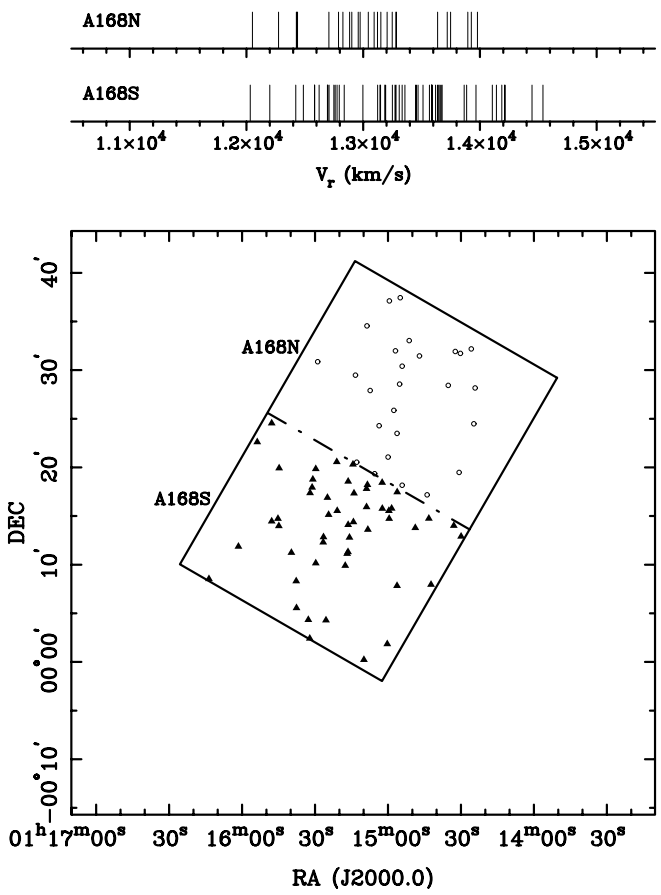

FIG. 8.—For the spectroscopically confirmed members in these two subclusters, the stripe density plot of velocity is plotted above the spatial distribution.

the cluster A98. Under this model, the relative velocity V and the separation R between two subclusters can be converted into the observational quantities: the relative radial velocity $V_r = V \sin\alpha$ and the projection separation $R_p = R\cos\alpha$. The projection angle α ($\in[0,\pi/2]$) is defined as the angle between the line connecting the two subclusters and the plane of sky. The energy relation for gravitational binding is taken from the Newtonian criterion

$$\frac{V_r^2 R_p}{2GM} \leq \sin^2\alpha\ \cos\alpha, \tag{2}$$

where G is the gravitational constant. M is the system mass, equal to the total mass of the two subclusters. The difference of mean velocity between A168N and A168S can be easily figured out $V_r = 264 \pm 142$ km s^{-1}. We take $R_p = 0.584$ Mpc, the distance between the two X-ray peaks that roughly represent the centers of these two subclusters. Following the method described in Beers et al. (1982), the mass and the gravitational scale lengths of A168N, A168S, and A168 are estimated and listed in Table 2. The probability of gravitational binding can be obtained by the formula

$$P = \frac{1}{A}\int_0^{+\infty} p(V_r)p(\alpha|V_r)dV_r\,, \tag{3}$$

where A is renormalization factor; $p(V_r)$ is the probability distribution of the velocity, which is assumed to be a Gaussian; $p(\alpha|V_r)$, which can be obtained from equation (2), is the probability of the valid α for gravitational binding at a given V_r. Integration is over all the appropriate values of velocity. As a result, we find that these two subclusters are gravitationally bound with a probability of 92%.

Another efficient statistic method to test the substructures of the radial velocity distribution was recently introduced by Colless & Dunn (1996), who keep the spirit of the Dressler-Shectman test (Dressler & Shectman 1988) and employ the standard K-S test to compare the velocity distribution of the local group, n nearest neighbors, and the whole velocity distribution. The statistic is defined as

$$\kappa_n = \sum_{i=1}^{N} -\log\left[P_{\rm KS}(D > D_{\rm obs})\right], \tag{4}$$

where N is the number of all member galaxies of a cluster and D is the statistic in standard K-S test. For each galaxy, we compute the probability, $P_{\rm KS}(D > D_{\rm obs})$, of its local group via Monte Carlo simulation by randomly shuffling velocities every time. This probability gives an indication of how significant the observed $D_{\rm obs}$ is by comparing with the simulations; κ_n is an indication that the local velocity is different from the overall distribution.

We take the group size of $n = 10$. By involving 10^5 simulations, we find that $\kappa_{10} = 0.000\%$, almost no simulated D greater than the observed $D_{\rm obs}$. A significant deviation of local velocity distribution from the overall distribution can be found in Figure 9. The bubble radius for each galaxy is proportional to $-\log\left[P_{\rm KS}(D > D_{\rm obs})\right]$. Consistent with the result of spectroscopic redshifts, no further substructure was found in the central region, because the photometric redshift is not precise enough to distinguish the small difference, such as ~ 260 km s^{-1}, in velocity. The result possibly suggests that the two subclusters are approaching each other along the plane perpendicular to our line of sight. The obvious bubble concentration at the west possibly supports the existence of the west group discussed in § 3.1.

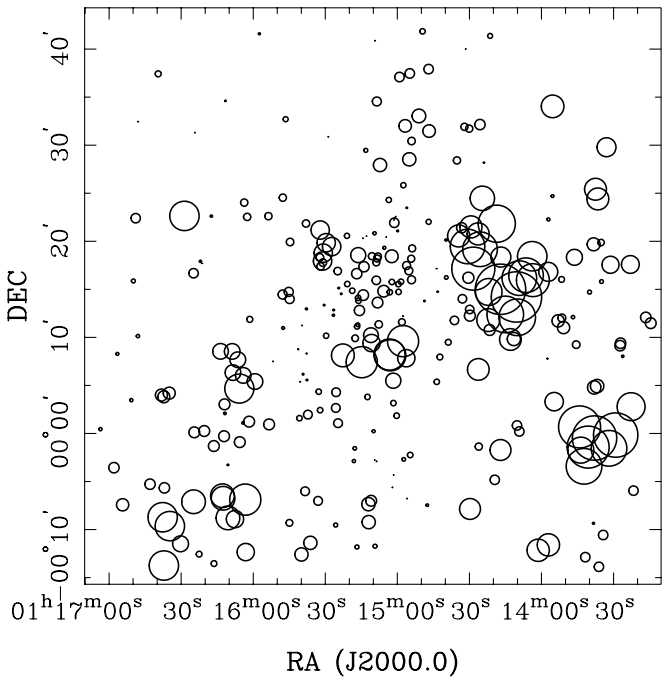

4. LUMINOSITY FUNCTIONS

4.1. *Double Schechter Function*

The luminosity function is a key diagnostic for clusters of galaxies because it is tightly related to the dynamical evolution and the merging history of galaxy clusters. In the past decades, the LFs of GCs have been well described by the famous Schechter function, which was originally proposed by Schechter (1976):

$$\phi(L)dL = \phi^*\left(\frac{L}{L^*}\right)^{\alpha}\exp\left(-\frac{L}{L^*}\right)d\left(\frac{L}{L^*}\right), \tag{5}$$

where ϕ^*, L^*, and α are the normalization parameter, the characteristic luminosity, and the faint slope parameter, respectively.

Recently, the deep observation of the Coma Cluster revealed that their LFs possess an enhanced faint tail (e.g., Trentham & Tully 2002). It is widely perceived that a single Schechter function gives a poor representation of the data when the LFs extend to the fainter end (Biviano et al. 1995; Durret et al. 1999; Trentham & Tully 2002). The segregation in LFs of GCs suggests that there are at least two populations of the galaxies in clusters (Durret, Adami, & Lobo 2002). For example, Ferguson & Sandage (1991) used a Gaussian part plus Schechter function in order to probe the two populations, the giants and the dwarfs.

The Schechter function works well for the bright end as shown in the previous literatures, such as Dressler (1978) and Paolillo et al. (2001). However, the present extending LFs require a variation to describe the enhanced tail rather than a

TABLE 3
FITTING RESULTS OF LFS OF A168

Region	ϕ_0^*	M_0^*	α_0	ϕ_1^*	M_1^*	α_1	$\chi^2_{\rm min}$
A168N.....	$14.9^{+3.4}_{-2.9}$	$-21.75^{+0.67}_{-2.50}$	$0.04^{+0.08}_{-0.07}$	$37.5^{+20.2}_{-15.9}$	$-16.91^{+0.56}_{-0.63}$	$0.40^{+0.98}_{-1.00}$	1.6
A168S	$54.4^{+8.5}_{-7.4}$	$-20.47^{+0.31}_{-0.40}$	$0.36^{+0.08}_{-0.08}$	0.00	...	...	3.4
A168N+S	$50.3^{+5.6}_{-5.2}$	$-21.14^{+0.32}_{-0.48}$	$0.05^{+0.04}_{-0.04}$	0.00	...	...	4.1
Total	$95.8^{+10.}_{-9.4}$	$-20.77^{+0.23}_{-0.30}$	$0.17^{+0.05}_{-0.05}$	$138.9^{+24.5}_{-22.6}$	$-17.48^{+0.19}_{-0.20}$	$-0.19^{+0.28}_{-0.26}$	3.6

NOTE.—The errors are computed at the 68% confidence level.

single Schechter function. Hence we propose an acceptable *double* Schechter function (DSF):

$$N(M) = \phi_0^*[10^{-0.4(M-M_0^*)}]^{\alpha_0} e^{10^{-0.4(M-M_0^*)}} + \phi_1^*[10^{-0.4(M-M_1^*)}]^{\alpha_1} e^{10^{-0.4(M-M_1^*)}} . \quad (6)$$

Each term has the same form as the Schechter function in equation (5): M_i^* $(i = 0,\ 1)$ is the characteristic absolute magnitude with an equivalent characteristic luminosity; ϕ_i^*, α_i $(i = 0,\ 1)$ have the same meanings as in equation (5).

4.2. *Luminosity Functions*

We use the DSF to fit the observed LFs by means of the χ^2 minimization. The results are listed in Table 3 and plotted in Figure 10. A168S shows a decay tail while A168N shows an increasing one, suggesting that the galaxy contents of these two regions are quite different. We also compute the ratio of bright galaxies ($M_{r'} \leq -18.5$) to faint galaxies ($M_{r'} > -18.5$) for these two subclusters. This ratio for A168N is found to be $32/47 = 0.68$. However, for A168S, the ratio is $56/41 = 1.37$. It is obvious that the bright galaxies are more abundant in A168S while the faint galaxies are more likely to occur in A168N. This can be interpreted by the cannibalism model (Hausman & Ostriker 1978). That is to say, the cD galaxies are likely to be formed by accreting the surrounding massive galaxies, which naturally results in the deficit of bright galaxies in the most dynamically evolved clusters (Lugger 1986). Hence, the formation and evolution of these two subclusters might be different. A168N, associated with the cD galaxy UGC 00797, is likely to be more evolved than A168S. To confirm that our division of A168N and A168S is not accidental, we try other methods of dividing the core region. For example, we divide the core region into an east and a west part equally along the elongated direction of the spatial distribution. In this case, the clear contrast in the LFs disappears, which supports that the division of A168N and A168S is a special choice and that they are the two subclusters under the merging event of A168.

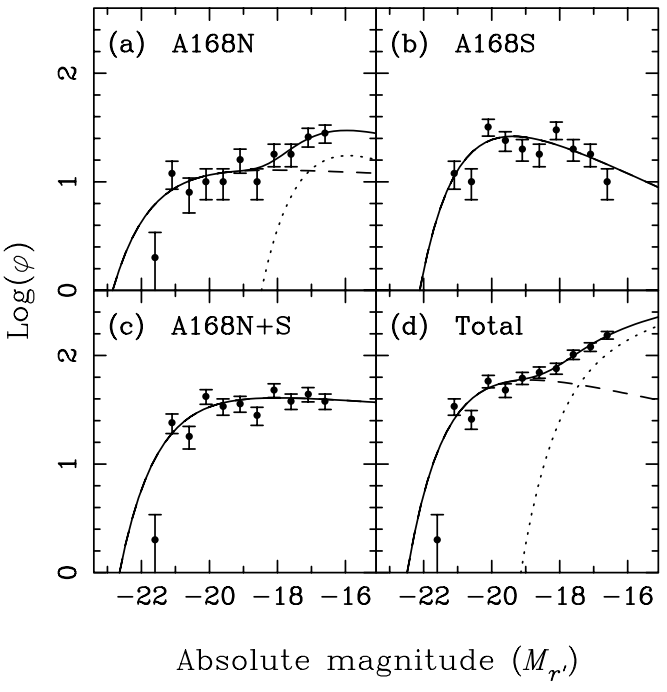

FIG. 10.—Observed luminosity functions fitted by DSF. The dashed lines and the dotted lines indicate the components of the DSF and the solid lines are their sum. Panels *a* and *b* are of the north subcluster and south subcluster, respectively. The LF of the central region is plotted in panel *c*. In panel *d* we show the LF of all 376 members in the whole field. For A168S and A168N+S (equal to the central region of A168), the single Schechter function gives a better representation than the DSF. The detailed discussion on LFs is made in § 4.2.

Figure 10*c* shows the LF of the central region (A168N+S) of the cluster. As shown in the previous works of Dressler (1978) and Oegerle et al. (1986), the LF has a quite flat tail, which is, however, an average of the LFs of A168N and A168S according to the present work. As for the whole field, the observed LF and its fitting model are shown in Figure 10*d*. For the overall LF, DSF gives a good description to the obvious enhanced faint tail at $M_{r'} > -18.5$ mag. Compared with the LF of the central region, the overall LF suggests that the faint galaxies (possible dwarfs) tend to be located in the outer region of the cluster. This perhaps supports the population-density relation: dwarfs are more common in lower density environments (Phillipps et al. 1998).

5. SUMMARY

We accumulated about 37 hours of high-quality observations of A168 with 13 intermediate filters of BATC photometric system. In the EDR of SDSS, we find that the photometry and the spectroscopic redshift measurement are completed in the same field. After a cross-identification with SDSS, we combine the photometric data of the objects detected in two systems resulting in the 18 band SEDs, which include 13 BATC bands and five SDSS bands. A complete sample of 1553 galaxies brighter than $r' = 20$ mag is achieved for the subsequent study.

By using the technique of photometric redshift, we get an enlarged sample of 376 galaxies, including 121 spectroscopically identified member galaxies and 255 newly selected member candidates. Spatially, the member galaxies show an elongated distribution along the northwest-southeast direction with a position angle of $\sim 30^\circ$, which is consistent with the spatial characteristic of the X-ray image obtained by *Einstein*.

Moreover, the two X-ray peaks and the deviation of the cD galaxy UGC 00797 from the local density peak support the existence of substructures in A168. According to the spatial characteristics, we artificially divide the core region into two parts, A168N and A168S. By employing ROSTAT software, a detailed investigation of the dynamics of these two subclusters is performed. A relative radial velocity of 264 ± 142 km s^{-1} was found between them. Their velocity distributions are intrinsically different and should be from the different parent distributions. Via building a linear two-body model, they are found to be gravitationally bound with a probability of 92%. Investigation of LFs by the DSF shows an obvious difference in the galaxy content of these two subclusters. A168S is dominated by bright galaxies, while A168N has larger number of faint galaxies. A168N is a subsystem associated with the cD galaxy and likely to be a more evolved system than A168S. All these indications are consistent and support that A168 is likely to be a head-on merging system at an early stage of the process and that the collision plausibly occurs along the direction perpendicular to our line of sight.

The authors would like to thank the referee Timothy Beers, who gave helpful suggestions for improving the paper. We are grateful to the following persons for their valuable suggestions and discussion: Dr. HaiGuang Xu, SuiJian Xue, XiangPing Wu, XiaoFeng Wang, Yu Liu, ZhengYu Wu, Mr. Yu Lu, Ms. Bin Yang, LiFang Xia, and especially Mr. Albrecht Rüdiger. We also appreciate the assistants who contributed their hard work to the observations. This research has made use of the NASA/IPAC Extragalactic Database (NED), the EDR of SDSS, and the High Energy Astrophysics Science Archive Research Center (HEASARC). This work is supported by the National Key Base Sciences Research Foundation (NKBRSF, TG199075402) and is also supported by the Chinese National Science Foundation (NSFC).

REFERENCES

Bahcall, N. A. 1988, ARA&A, 26, 631
Beers, T. C., Flynn, K., & Gebhardt, K. 1990, AJ, 100, 32
Beers, T. C., & Geller, M. J. 1983, ApJ, 274, 491
Beers, T. C., Geller, M. J., & Huchra, J. P. 1982, ApJ, 257, 23
Bird, C. M., & Beers, T. C. 1993, AJ, 105, 1596
Biviano, A., Durret, F., Gerbal, D., Le Fevre, O., Lobo, C., Mazure, A., & Slezak, E. 1995, A&A, 297, 610
Bolzonella, M., Miralles, J.-M., & Pelló, R. 2000, A&A, 363, 476
Colless, M., & Dunn, A. M. 1996, ApJ, 458, 435
Dressler, A. 1978, ApJ, 223, 765
———. 1984, ARA&A, 22, 185
Dressler, A., & Gunn, J. E. 1988, in IAU Symp. 130, Large Scale Structures of the Universe, ed. J. Audouze et al. (Dordrecht: Kluwer), 311
Dressler, A., & Shectman, S. A. 1988, AJ, 95, 985
Durret, F., Adami, C., & Lobo, C. 2002, A&A, 393, 439
Durret, F., Gerbal, D., Lobo, C., & Pichon, C. 1999, A&A, 343, 760
Fan, X.-H., et al. 1996, AJ, 112, 628
Ferguson, H. C., & Sandage, A. 1991, AJ, 101, 765
Forman, W., & Jones, C. 1982, ARA&A, 20, 547
Hausman, M. A., & Ostriker, J. P. 1978, ApJ, 224, 320
Jones, C., Mandel, E., Schwarz, J., Forman, W., Murray, S. S., & Harnden, F. R. 1979, ApJ, 234, L21
Kriessler, J. R., & Beers, T. C. 1997, AJ, 113, 80
Lugger, P. M. 1986, ApJ, 303, 535
Oegerle,W. R., Ernst, R. M., & Hoessel, J. G. 1986, AJ, 91, 697
Oegerle, W. R., & Hill, J. M. 2001, AJ, 122, 2858
Paolillo, M., Andreon, S., Longo, G., Puddu, E., Gal, R. R., Scaramella, R., Djorgovski, S. G., & de Carvalho, R. 2001, A&A, 367, 59
Pelló, R., et al. 1999, A&A, 346, 359
Phillipps, S., Driver, S. P., Couch, W. J., & Smith, R. M. 1998, ApJ, 498, L119
Poggianti, B. M. 2002, preprint (astro-ph/0210233)
Schechter, P. 1976, ApJ, 203, 297
Schindler, S. 2001, preprint (astro-ph/0109040)
Stoughton, C., et al. 2002, AJ, 123, 485
Tomita, A., Nakamura, F. E., Takata, T., Nakanishi, K., Takeuchi, T., Ohta, K., & Yamada, T. 1996, AJ, 111, 42
Trentham, N., & Tully, R. B. 2002, MNRAS, 335, 712
Ulmer, M. P., Wirth, G. D., & Kowalski, M. P. 1992, ApJ, 397, 430
Xia, L., et al. 2002, PASP, 114, 1349
Yuan, Q., Zhou, X., Chen, J., Jiang, Z., Ma, J., Wu, H., Xue, S., & Zhu, J. 2001, AJ, 122, 1718
Yuan, Q., et al. 2003, ApJS, 149, 53
Zhou, X., Chen, J., Xu, W., Zhang, M., Jiang, Z., Zheng, Z., & Zhu, J. 1999, PASP, 111, 909
Zhou, X., Jiang, Z., Xue, S., Wu, H., Ma, J., & Chen, J. 2001, Chinese J. Astron. Astrophys., 1, 372
Zhou, X., et al. 2003, A&A, 397, 361